# Exploring Reduction Strategies for Polarimetric Imaging with FORS2

João Rino-Silvestre, PhD program (PD/BD/150487/2019), integrated in the CRISP project (PTDC/FIS-AST/31546/2017)
Advisors: Santiago González-Gaitán, Ana Mourão

## Dual-Beam Polarimetry

Dual-Beam polarimetry is an observational technique that exploits the birefringence (the optical property of a material having a refractive index that depends on the polarization and propagation direction of light) of some materials to measure the polarization of target sources by splitting the observed light into two beams of complementary polarization states, the ordinary beam, $f_o$, (with polarization perpendicular to the optical axis of the material) and the extra-ordinary beam, $f_e$ (with polarization parallel to the optical axis).

FORS2 polarimetric imaging setup is composed by the usual focal optics and CCD but has in-between these two systems two other components, a half-wave plate (HWP) and a Wollaston prism (WP). The HWP causes a half-wave retardation between the polarization components of the wave, causing the polarization vector to be reflected along the HWP optical axis, while the WP spatially splits the two polarization components of the wave at its junction, due to having different refraction indexes for their respective directions (see Fig. 1). Two beams are hence detected.

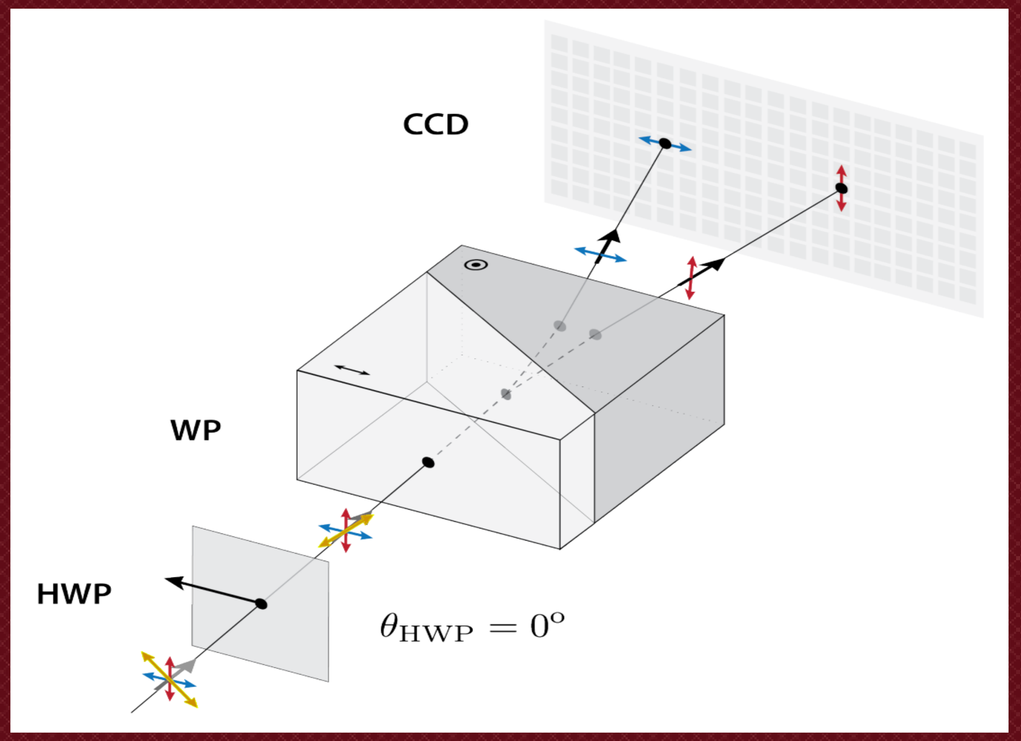


*Fig. 1: Schematic representation of the impact of a HWP and a WP on a lightwave that traverses them before being detected. The HWP causes a half-wave retardation between the polarization components of the wave, causing the polarization vector (in yellow/orange) to be reflected along the HWP optical axis. The WP spatially splits the two polarization components of the wave at its junction due to having different refraction indexes for their respective directions. At the CCD in red we can see the extra-ordinary beam, and in blue the ordinary beam (image adapted from González-Gaitán, Mourão et al. 2020).*

The beams are measured four times, each time with the HWP optical axis at a different angle, $\theta_i \in \{0^o, 22.5^o, 45^o, 67.5^o\}$. These measurements are then combined to recover Stokes linear polarization parameters (Q and U) of the observation. There are two ways to do this, the difference method, see Eq. (1), and the ratio method, see Eq. (2). The polarization degree and angle, P and χ, are then calculated using Eq. (3).

$$F_i \equiv \frac{f_o^i - f_e^i}{f_o^i + f_e^i} \qquad \bar{Q} = \frac{2}{N}\sum_{i=0}^{N-1} F_i \cos\frac{\pi}{2}i \qquad \bar{U} = \frac{2}{N}\sum_{i=0}^{N-1} F_i \sin\frac{\pi}{2}i \tag{1}$$

$$R_i \equiv \frac{f_o^i}{f_e^i} \qquad \bar{Q} = \frac{\sqrt{\frac{R_0}{R_2}} - 1}{\sqrt{\frac{R_0}{R_2}} + 1} \qquad \bar{U} = \frac{\sqrt{\frac{R_1}{R_3}} - 1}{\sqrt{\frac{R_1}{R_3}} + 1} \tag{2}$$

$$P = \sqrt{\bar{Q}^2 + \bar{U}^2} \qquad \chi = \frac{1}{2}\arctan\frac{\bar{U}}{\bar{Q}} \tag{3}$$

## Testing on a Simulated Case

A square object of 20×20 pixels and homogeneous flux of 1000 ADU is defined, with polarization degree 1 (in a scale of 0 to 1) overall positions. Each pixel is set to a different polarization angle, spanning from 0° to 90° (see Fig. 2).

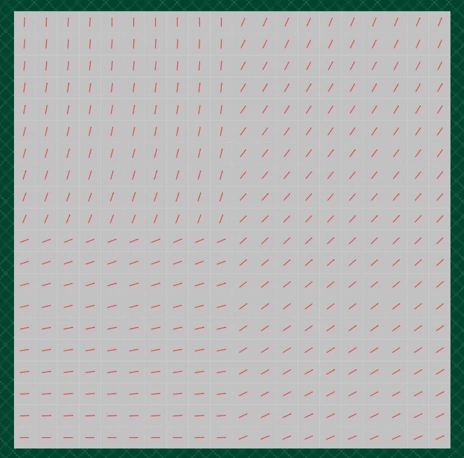

*Fig. 2: Simulated object. Homogeneous 1000 ADU flux, and polarization degree 1. Each pixel has a different polarization angle, spanning from 0° to 90°.*

Then the object's light flux is simulated going through an HWP four times. Each time the HWP optical axis is angled differently at 0°, 22.5°, 45° and 67.5°. The interaction with the HWP causes a phase difference between the two orthogonal polarization components, which results in a change of the polarization state of the outcoming light and conversely for each HWP angle, different ordinary and extra-ordinary beam fluxes.

The simulation continues with the light going through the WP, which spatially separates the two beams. In this step a non-homogeneous polarization flat (WP) is simulated, that attenuates extra-ordinary beam by 30% and ordinary beam by 80%.

Lastly, the beams are detected by the CCD. At this stage the CCD flat is simulated (see Fig. 3, with different detecting sensitivities for each pixel of the CCD, these sensitivities are modeled by a Gaussian distribution with μ = 0 and σ = 0.3.

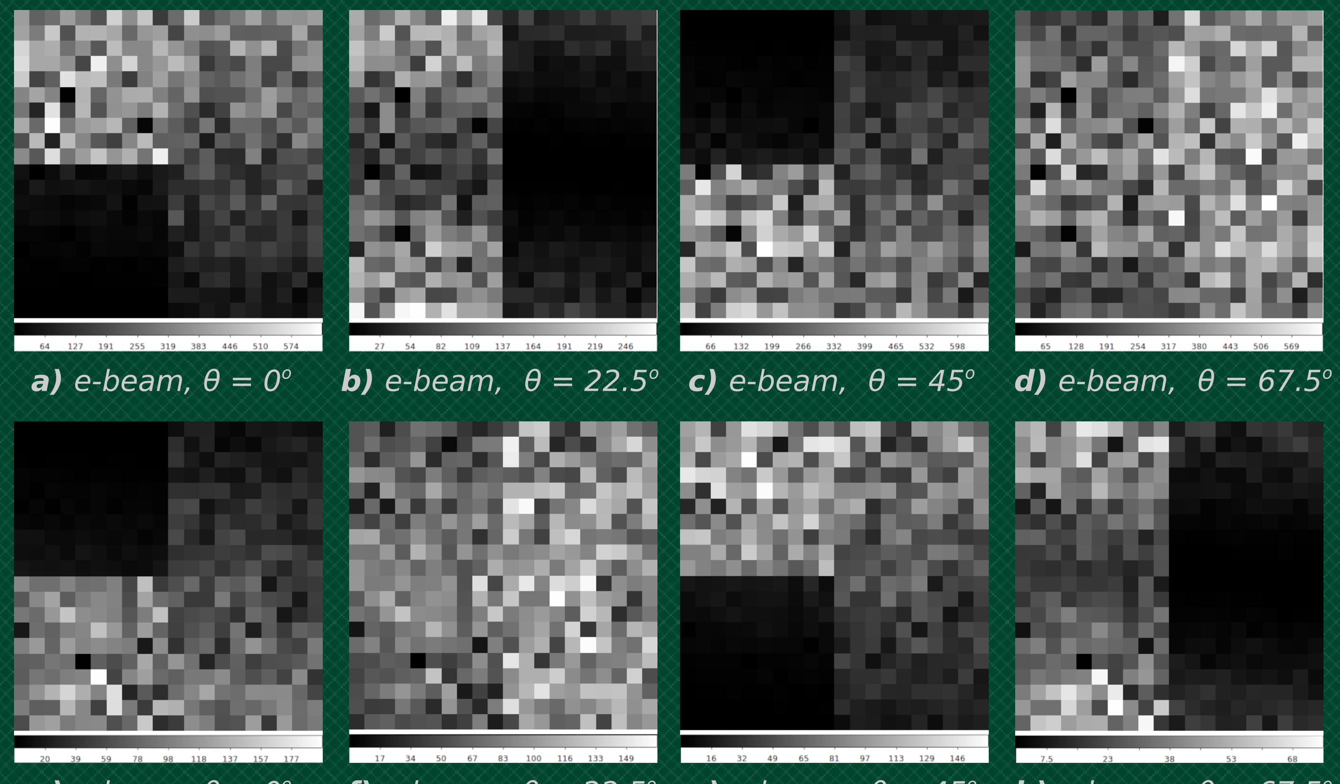

**a)** e-beam, θ = 0° **b)** e-beam, θ = 22.5° **c)** e-beam, θ = 45° **d)** e-beam, θ = 67.5°

**e)** e-beam, θ = 0° **f)** e-beam, θ = 22.5° **g)** e-beam, θ = 45° **h)** e-beam, θ = 67.5°

*Fig. 3: Beams detected by the CCD. In a) to d), extra-ordinary beam measured with HWP optical axis at 4 different angles, $\theta_i$. In e) to h), ordinary beam measured with HWP optical axis at the same 4 angles.*

*Tab. 1: Normalized residuals for the calculation of P, χ, Q and U, using 2 different methods and assuming 4 distintc scenarios.*

| Method | Scenario | Residuals (%) | | | | | | | |
|---|---|---|---|---|---|---|---|---|---|
| | | $P$ | | $\chi$ | | $Q$ | | $U$ | |
| | | $\mu$ | $\sigma$ | $\mu$ | $\sigma$ | $\mu$ | $\sigma$ | $\mu$ | $\sigma$ |
| Difference | RAW | 12 | 16 | 0 | 0 | 12 | 16 | 12 | 16 |
| | IF | 9 | 9 | 0 | 0 | 9 | 9 | 9 | 9 |
| | PF | 2 | 4 | 0 | 0 | 2 | 4 | 2 | 4 |
| | IPF | 0 | 0 | 0 | 0 | 0 | 0 | 0 | 0 |
| Ratio | RAW | 0 | 0 | 0 | 0 | 0 | 0 | 0 | 0 |
| | IF | 0 | 0 | 0 | 0 | 0 | 0 | 0 | 0 |
| | PF | 0 | 0 | 0 | 0 | 0 | 0 | 0 | 0 |
| | IPF | 0 | 0 | 0 | 0 | 0 | 0 | 0 | 0 |

We then calculate Q and U, using the difference and the ratio methods, and recover P and χ. Four scenarios were considered: without accounting for the impact of the CCD nor of the WP (RAW), accounting only for the CCD (IF), only for the WP (PF), and accounting for both CCD and WP (IPF). The residuals of each calculation (see Tab. 1) compared to the original object show that the ratio method is a more robust agnostic tool.

## Testing on FORS2 Data

We then took polarimetric imaging data of NGC1404, from FORS2 instrument of the Very Large Telescope, to test the two calculation methods on (see Fig. 4). The data was median-binned with bins of size 30×30 pixels (the white stripes that can be seen in this section's images are due to the polarization filter mask that is applied on the CCD to avoid an overlap of extra-ordinary beam and ordinary beam of different spatial regions, which results in only half the lightfield being measured).

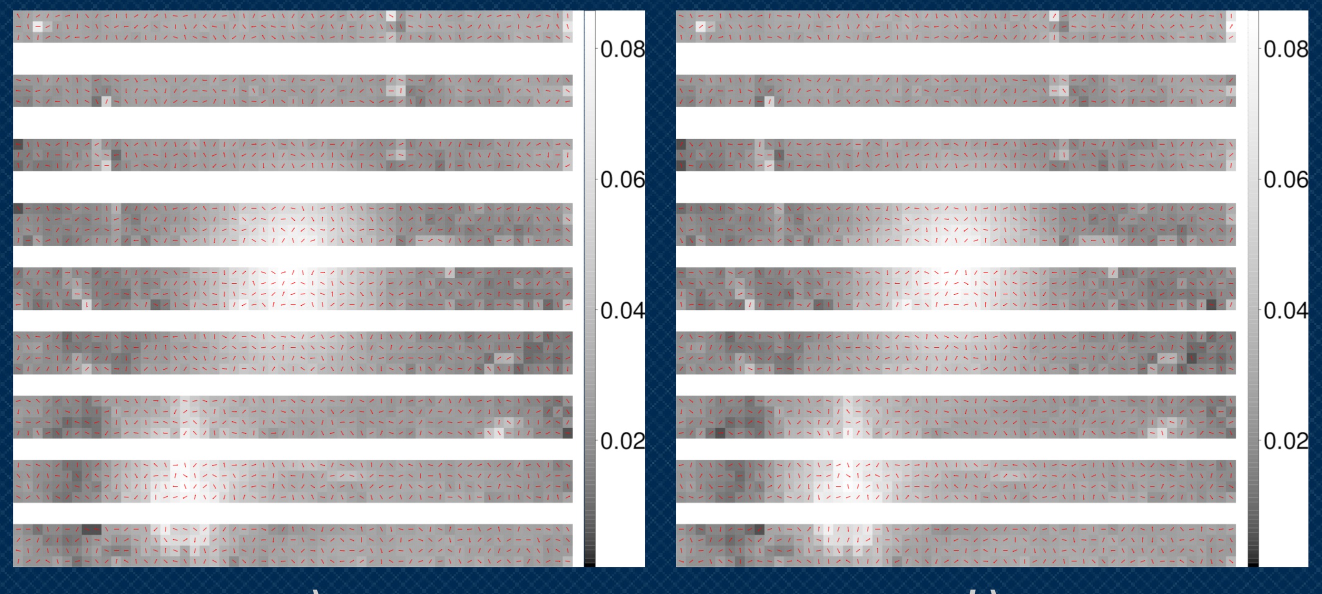


**a)** **b)**

*Fig. 4: Preliminary polarization maps for NGC1404, using FORS2 polarimetric imaging data measured in B band, calculated using the a) difference method, and b) ratio method. In each map the color of the pixels indicate the polarization degree, P, while the red line tilt indicates the polarization angle, χ.*

The absolute residuals of the results (see Fig. 5) show a median offset between the two methods of ΔP ~ 0.02 and Δχ ~ 33°, where the median values calculated are in the order of P ~ 0.01 and χ ~ 5°.

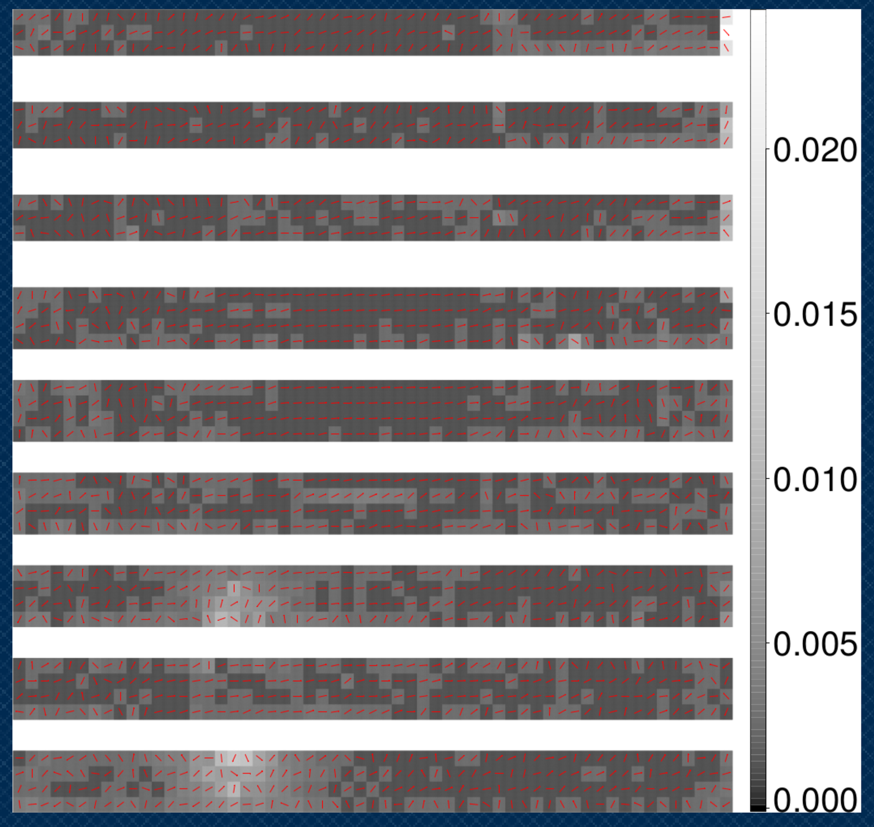


*Fig. 5: Absolute residuals calculated between the polarization degree and angle obtained using the difference and the ratio methods. The color of the pixels indicate the absolute residual of polarization degree, ΔP, while the red line tilt indicates the absolute residual of polarization angle, Δχ.*

This shows that the ratio method can greatly improve the quality of polarimetric measurements, likely due to being inherently robust to possible unhomogeneity of the WP (see Tab. 1). This can be used to improve the estimation of local interstellar polarization corrections to the polarization analysis of supernovae.